



The ZEUS microvertex detector

C. Coldewey

for the ZEUS Microvertex Group

DESY, Platanenallee 6, D-15738 Zeuthen, Germany

Abstract

For the HERA luminosity upgrade in the year 2000, the ZEUS experiment is preparing a high-precision vertex detector using single-sided silicon microstrip detectors with capacitive charge division. The readout pitch of the detectors is 120 μm with five intermediate strips. The paper reviews the design of the microvertex detector consisting of a central part with three double layers and four wheels in the forward region. Results on electrical measurements before and after irradiation on the detectors and on the test structures designed for quality-control measurements are presented. For a number of prototype detectors mounted to the prototype readout electronics (HELIX-128) the pulse height distribution and the position resolution has been measured in a test beam using 6 GeV electrons. The expected position resolution of about 7.5 μm at normal incidence has been achieved. © 2000 Elsevier Science B.V. All rights reserved.

1. Introduction

Silicon strip detectors are successfully used in high-energy experiments for precise vertex determination, especially for the reconstruction of secondary vertex tracks, coming from the decay of heavy flavour particles or τ -leptons with a lifetime of about 10^{-12} s. A microvertex detector using silicon strip detectors is presently being constructed for the ZEUS experiment operating at the hadron electron ring collider HERA, located at DESY in Hamburg, Germany. HERA provides colliding beams of electrons, with an energy of 27.5 GeV, and protons of 920 GeV, corresponding to a centre-of-mass energy of 318 GeV. A detailed description of the ZEUS detector is given elsewhere [1]. Charged particles are measured by the inner tracking

detectors which operate in a magnetic field of 1.43 T provided by a thin superconducting coil. Around the beam pipe is the central tracking detector (CTD), which consists of 72 cylindrical drift chamber layers, organized into nine superlayers covering the polar angular region $15^\circ < \theta < 164^\circ$.¹ The energy measurement is performed with the high-resolution depleted-uranium calorimeter which covers the pseudorapidity region $4.3 > \eta > -3.8$.²

With the luminosity upgrade [2] during the shutdown starting in year 2000, the HERA program will enter an era of high sensitivity to low e-p cross-section physics. To take advantage of the larger statistics, ZEUS will install the silicon

¹ The polar angle θ is defined with respect to the proton beam direction.

² $\eta = -\log \tan(\theta/2)$.

E-mail address: coldewey@mail.desy.de (C. Coldewey).

microvertex detector, MVD, prior to the high luminosity running. The need of a microvertex detector is well motivated [3]. Beside a general improvement of the track reconstruction, physics topics like the identification of heavy flavour events via secondary vertices or the identification of high Q^2 neutral current events with scattered electrons close to the beamline will profit from the improved vertex finding and the extended angular coverage in the forward region.

2. Microvertex detector design

The MVD consists of a central (BMVD) and a forward (FMVD) detector. Fig. 1 shows a cross section of the MVD with the four wheels of the FMVD located at $z = 311, 441, 571$ and 721 mm from the interaction point, and the three double layers of the BMVD in the central region.

2.1. The FMVD layout

The forward vertex detector with four wheels covers the acceptance for track reconstruction from $\eta = 1.8$ to 2.6 , a region not covered by the existing tracking system. A cross section of a wheel perpendicular to the beam line is shown in Fig. 2.

Each wheel is made of 14 FMVD readout cells, which consist of two wedge-shaped strip detectors behind each other. The shape of the detectors is shown in Fig. 3. The top and bottom sides are parallel to each other, while the other two sides are tilted by $\pm 13^\circ$. A detector has 480 readout strips which are parallel to one of the tilted sides. Using

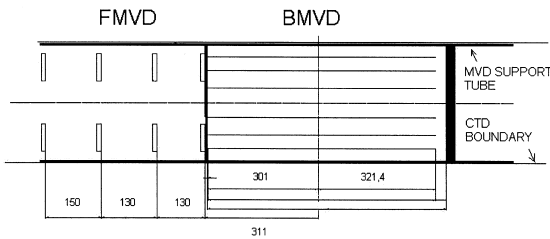


Fig. 1. Layout of the MVD along the beam line with different horizontal and vertical scales. Shown are the four wheels of the FMVD and the three double layers parallel to the beam line in the central region.

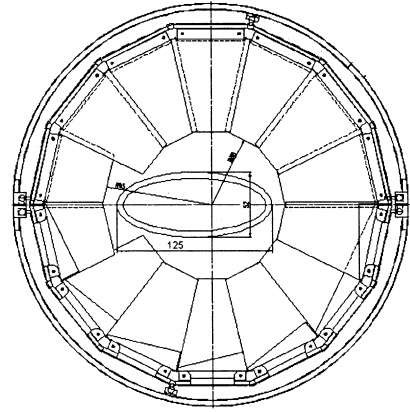


Fig. 2. Layout of the FMVD perpendicular to the beam line.

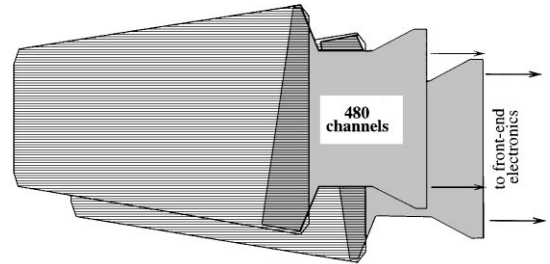


Fig. 3. FMVD readout cell consisting of two wedge-shaped strip detectors.

two overlapping detectors with oppositely tilted strips, a readout cell allows the measurement of r and ϕ coordinates simultaneously. The FMVD and BMVD detectors are using the same technology and are produced by Hamamatsu Photonics. A description of the electrical properties is given below, where the BMVD detector performance will be discussed.

Due to the elliptical shape of the beam pipe, two different types of wedge shapes are designed to optimize the coverage around the beam pipe, as shown in Fig. 2. Because of the synchrotron radiation, the beam pipe is not centered with respect to the CTD axis and the nominal interaction point is shifted by about 4 mm towards the HERA center.

Each readout channel is connected via a multi-strip-polymide (Upilex³) cable with the front-end

³ Polyimid product of UBE Technologies Ltd, Japan.

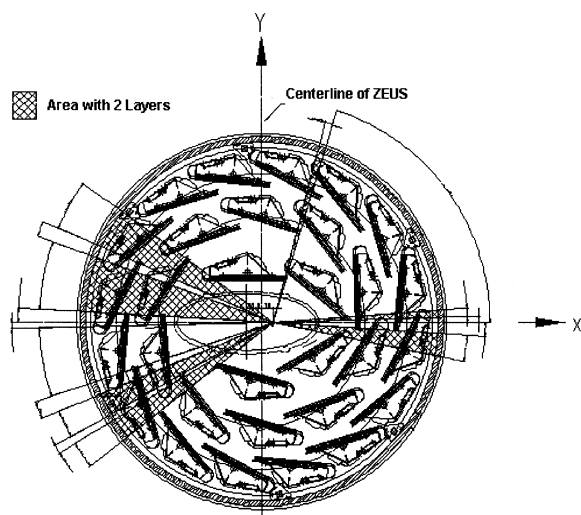


Fig. 4. Layout of the BMVD perpendicular to the beam line.

electronic consisting of HELIX 3.0 [4,5] chips with 128 integrated channels. For a description of the readout electronics see Ref. [6].

2.2. The BMVD layout

The BMVD is made of 600 strip detectors mounted on 30 carbon fibre support structures, the so-called ladders, with two layers of detectors arranged with strips parallel and perpendicular to the beam line for r - ϕ and r - z measurements. A cross section of the BMVD showing the position of the ladders in the r - ϕ plane is given in Fig. 4. Depending on the azimuth angle, the first layer of detectors is placed at a distance of 3–5 cm from the CTD axis followed by second and third layers at about 8.6 and 12.3 cm, respectively. Regions in ϕ covered by two double layers only are indicated by the dashed areas.

2.3. BMVD detector design

The BMVD microstrip detectors are made of $64 \text{ mm} \times 64 \text{ mm} \times 330 \text{ }\mu\text{m}$ high-resistivity 3–6 $\text{k}\Omega \text{ cm}$ n-type silicon with implanted p^+ strips at a pitch of $20 \text{ }\mu\text{m}$. There are 512 readout strips with 5 intermediate strips in between, resulting in a pitch of $120 \text{ }\mu\text{m}$ for the readout strips. The strips

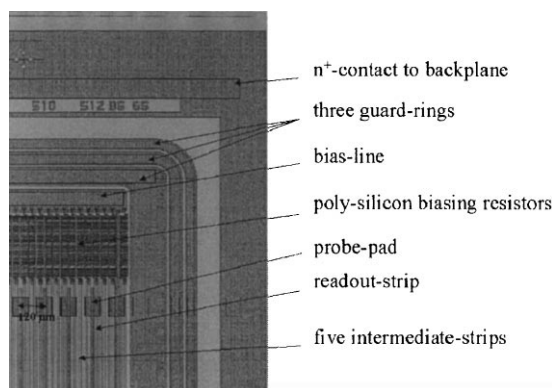


Fig. 5. A view of one corner of the BMVD strip detector.

have a length of 62.4 mm and a width of 12 and $14 \text{ }\mu\text{m}$ for intermediate and readout strips, respectively. The readout strips are covered by aluminium lines of $12 \text{ }\mu\text{m}$ width isolated from the p^+ strips by a double layer of SiO_2 and Si_3N_4 for AC coupling. The biasing of the p^+ strips is implemented using poly-Si resistors which alternately connect even and odd strips to bias lines placed near the detector edges (see Fig. 5). The entire set of strips is encircled by three guard rings with widths of 100, 65 and $55 \text{ }\mu\text{m}$, going from the inner to the outer guard rings.

Capacitive charge division is used between the readout strips in order to limit the number of readout strips and achieve a spatial resolution of about a $10 \text{ }\mu\text{m}$ for particles traversing the detector with angles up to 30° with respect to the surface. By means of capacitive coupling between strips, the charge collected at intermediate strips induces charges on the readout strips which are approximately inversely proportional to the distance between interpolation and readout strips [7]. Uniformity in charge collection can be achieved keeping all the strips (readout and intermediate) at the same potential using bias resistors for every strip. Charge losses to the backplane are minimized by imposing the interstrip capacitance much larger than the capacitance to the detector backplane.

2.4. The BMVD ladder

The BMVD detector module consists of four detectors arranged in two layers with strips parallel

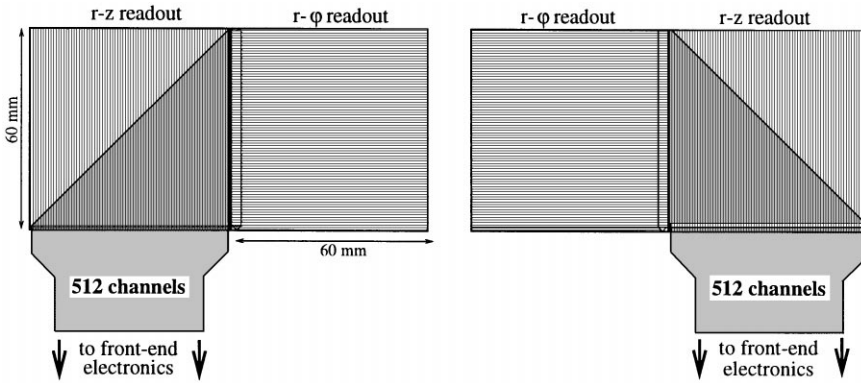


Fig. 6. The two readout cells of a BMVD module.

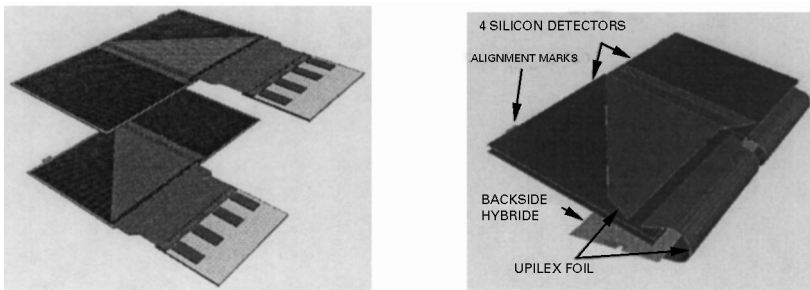


Fig. 7. The two readout cells of a BMVD module and a module ready for mounting.

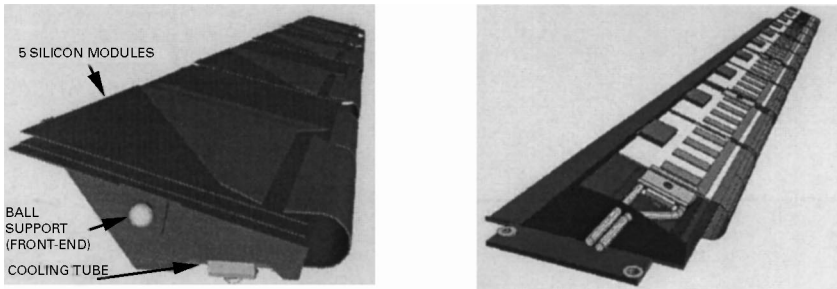


Fig. 8. Top and bottom view of fully assembled support ladders.

and perpendicular to the beam direction to allow $r-\phi$ and $r-z$ measurements as shown in Fig. 6. The two detectors of a layer are glued together with an overlap of 2 mm in the sensitive area, forming a readout cell of approximately $120 \times 60 \text{ mm}^2$. Each strip of a $r-z$ detector is connected with a corresponding strip of the $r-\phi$ detector via an Upilex foil cable of triangular shape as indicated in Fig. 6.

The connection scheme is chosen in such a way that for both layers the most outer strip of the $r-z$ detector will be connected with the most upper strip of the $r-\phi$ detector. An additional fanout foil, glued to the $r-z$ detector is used to connect the strips with the front-end electronics.

Fig. 7 shows the arrangement of two readout cells with the HELIX-128 front-end chips before

mounting them to a BMVD module. The complete module with 1024 channels is given in the right drawing of Fig. 7 with the bent Upilex foil, which allows one to place the front-end electronics below the detector. Two views of a completely mounted ladder are presented in Fig. 8. Five BMVD modules are placed on a ladder resulting in a length of 60 cm. On the right drawing of Fig. 8 one can also see the cooling pipes close to the front-end electronics.

3. Detector performance

A comprehensive test program is under way to understand the performance and main characteristics of the silicon strip detectors. In the following we will discuss five points of the program:

- *Test beam measurements:* A number of prototype detectors has been mounted to the prototype front-end electronics. The signal-to-noise ratio, the position resolution and the charge collection as function of the distance between the readout strips and the test beam position have been measured in a particle beam using 2–6 GeV electrons for incident angles between 0° and 70° .
- *Quality control measurements:* Main characteristics of the strip detectors like the full depletion voltage and the diode leakage current are measured for each detector.
- *Long-term test:* Each detector is biased at 200 V at least for 42 h, while the leakage current is monitored as function of the time. This measurement is an essential test to check the long-term stability.
- *Test structure measurements:* Test structures designed for quality control measurements are used to extract relevant process parameter, which cannot be measured directly on the detectors.
- *Irradiation tests:* The MVD detector is planned to operate for at least 5 yr of HERA running during which an integrated radiation dose of 300 Gy is anticipated. For safety reasons the MVD is defined to stand radiation doses up to 3 kGy without major performance degradation. At the position of the microvertex detector, H1 has measured a dose of 50 Gy for the 1996 data taking period. In order to estimate the radiation

hardness, strip detectors and test structures have been irradiated with neutrons and ionizing radiation using a ^{60}Co source.

3.1. Test beam measurements

To understand and verify the performance of the detectors and the readout electronics, a test beam has been setup. Prototype detectors assembled with the prototype readout electronics are being exposed to an electron beam of 2–6 GeV of the DESY II accelerator. The tracks of charged particles are measured by three pairs of reference detectors providing x and y coordinates. The reference detectors are strip detectors with 50 μm readout pitch and one intermediate strip. The accuracy in predicting the coordinates of the track is determined by the intrinsic resolution of the reference detectors and by multiple scattering. It has been measured as $\sigma = 5.4 \mu\text{m}$ for a 6 GeV electron beam. The main results of the test beam measurements are:

- A signal-to-noise ratio of $S/N \approx 22$ has been achieved for a single BMVD detector assembled with the prototype front-end electronics (HELIX-128 V2.2).
- Fig. 9 shows for 6 GeV electrons at normal incidence the difference between the position predicted by the beam telescope minus the position measured by the detector. Correcting for the 5.4 μm uncertainty of the predicted position results in a resolution of 7.5 μm .
- The mean charge collected as function of the particle position relative to the readout strips shows the expected behaviour (see Fig. 9). It follows the linear relation

$$Q_L = \frac{Q_0}{1 + 2\varepsilon} \cdot \left(\frac{x}{d} + \varepsilon \right)$$

and

$$Q_R = \frac{Q_0}{1 + 2\varepsilon} \cdot \left(\frac{d - x}{d} + \varepsilon \right)$$

with $\varepsilon \simeq 0.14$, where Q_L and Q_R denote the mean collected charge of the left and right strips of two neighbouring readout strips and d is the readout pitch.

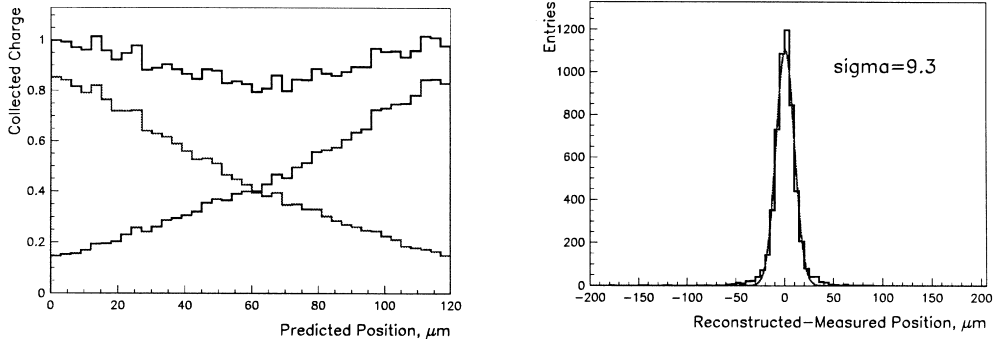


Fig. 9. The left plot shows the collected charge as function of the particle position, where 0 and 120 μm at the x-axis indicate the position of the centres of two neighbouring readout strips. Shown are the collected charge of two neighbouring readout strips separately and the sum of both curves. At the right plot the detector resolution is given.

3.2. Quality control measurements

The main electrical parameters have been measured on a probe station to verify that the detector behaves as designed. C - V curves and I - V curves were measured to determine the depletion voltage, V_{dep} and leakage currents I_{bias} . A combined voltage source and pico-amperemeter Keithley 487 is used to bias the detector during I - V and C - V measurements. For the C - V measurement a Hewlett Packard 4263A LCR meter is used. Possible measurement frequencies are 120 Hz, 1, 10 and 100 kHz. The resolution is 1 fF at 10 kHz.

3.2.1. I - V measurements

Fig. 10 shows the distribution of the detector leakage current measured at $V_{\text{bias}} = 200$ V for the first 240 detectors. Most of the detectors have small leakage currents below 100 nA, much smaller than the specified upper limit of 2 μA .

3.2.2. C - V measurements

The total bulk capacitance of the detector depends both on geometrical and electrical properties. Main parameters obtained from the C - V measurement are the full depletion voltage and the minimum bulk capacitance (C_{dep}) at bias voltages above full depletion. For measuring the total bulk capacitance, the first guard ring was grounded and the bias voltage was applied between the detector backplane and the bias line. After measuring the first 240 detectors, two types of detectors are

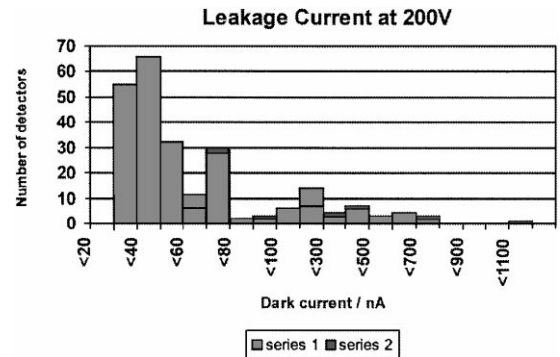


Fig. 10. Detector leakage current distribution measured at $V_{\text{bias}} = 200$ V.

observed, one with full depletion values of $V_{\text{dep}} \approx 62 \pm 3$ V and a second group with values between $V_{\text{dep}} = 43$ V and $V_{\text{dep}} = 52$ V. The deviation can be explained by different doping concentrations of the n^- substrate. Above full depletion we measured for all detectors a minimum bulk capacitance of $C_{\text{dep}} = 1.36$ nF at the default measurement frequency of 10 kHz, in reasonable agreement with the geometric capacitance $C_{\text{geom}} = \epsilon_0 \epsilon_{\text{Si}} \cdot A/d = 1.28$ nF, where $A = 63.4 \times 63.2$ mm² and $d = 330$ μm denote the effective size and thickness of the detector.

3.3. Long-term test

In order to test the long-term stability of the detectors, each detector is biased with

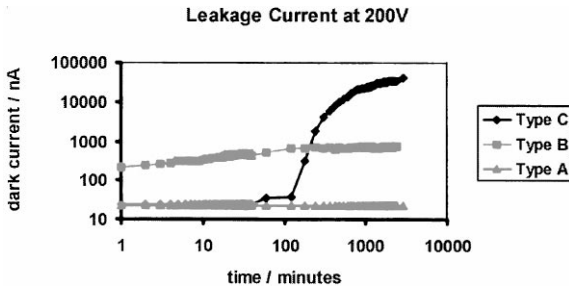


Fig. 11. Detector leakage current as function of time biased with $V_{\text{bias}} = 200$ V.

$V_{\text{bias}} = 200$ V for approximately 42 h. In Fig. 11 the detector leakage current as function of time is shown for three detectors. As shown in Fig. 11 three types are introduced for a long-term stability classification. Type-A detectors are represented by the lower curve with almost constant leakage currents over the full period of time and values of $I_{\text{leak}} \approx 20\text{--}50$ nA. While type-B detectors are still acceptable, there are detectors with a long-term behaviour as shown for the type-C curve, which would lead to an unpredictable behaviour during running time. After performing the long-term test for 59 detectors, we classified 30 type-A, 27 type-B and 2 type-C detectors.

3.4. Test structure measurements

Test structure measurements are an essential source for information not directly accessible from silicon detector. Test structures provide the possibility to obtain process relevant parameter, thus allowing one to control the production of the full detector series. Each detector is produced with a test structure field on the same wafer allowing a one to one correlation between a certain detector and its corresponding test structures.

The usability of test structures on high resistivity silicon has been widely investigated both theoretically and experimentally [8–10]. To control the most relevant process parameter the following structures were designed.

- 10 poly silicon resistors of the same layout as used for the detector with probing contacts on each side are available to control the poly silicon

resistance. The measured values were between $R_{\text{poly}} = 1.5$ and 2.5 M Ω . However, the spread of the resistance values for resistors of the same wafer was always below ± 0.1 M Ω .

- Since the p^+ resistance of readout and intermediate strips cannot be measured directly on the detector, two corresponding strips with implant widths of 14 and 12 μm and a length of 4.6 mm are placed on the test structures. The measured values of $R_{14} = 88$ k Ω/cm and $R_{12} = 102$ k Ω/cm scale precisely with the width of the strips. Assuming a depth of the p^+ implant of 0.1 μm and a hole mobility for highly doped material of $\mu_h = 80$ $\text{cm}^2 \text{V}^{-1} \text{s}^{-1}$ [9], one obtains a doping concentration of $N_{p^+} = 3 \times 10^{19} \text{cm}^{-3}$.
- Measurements on aluminium strips are possible. However probe pads on both sides of the readout strips allow direct measurements on the detector. The measured Al resistance of the readout strips is $R_{\text{Al}} \approx 20$ Ω/cm .
- A MOS capacitor provides the possibility for C – V measurements. The isolation layer is made of field oxide, which is the oxide placed between the p^+ strips on the detector. Measurements performed on the MOS field capacitance provide information on the oxide and the surface between the p^+ strips. An important quantity is the flatband voltage. The flatband voltage V_{fl} is strongly related to the density of oxide and interface charges. The effective surface charge density is given by $Q_{\text{ox}} = -(V_{\text{fl}} - \phi_{\text{ms}})C_{\text{ox}}$ where C_{ox} is the oxide capacitance per unit area and $\phi_{\text{ms}} \approx -1.0$ V is the work function difference between aluminium and silicon. The oxide capacitance is given by the capacitance value measured in accumulation, which in addition is a direct determination of the field oxide thickness via $t_{\text{ox}} = \epsilon_0 \epsilon_{\text{SiO}_2} \cdot 1/C_{\text{ox}}$. The measured thickness is $t_{\text{ox}} \approx 600$ nm. For unirradiated capacitors, we obtained a flatband voltage of $V_{\text{fl}} = -8.3$ V which corresponds to about 3×10^{11} charged states/ cm^2 .
- PMOS field transistors with different W/L ratios can be used to study the decrease of the hole mobility due to irradiation.
- A readout strip with probing pads for the p^+ and the Al strip allows to control the quality of the

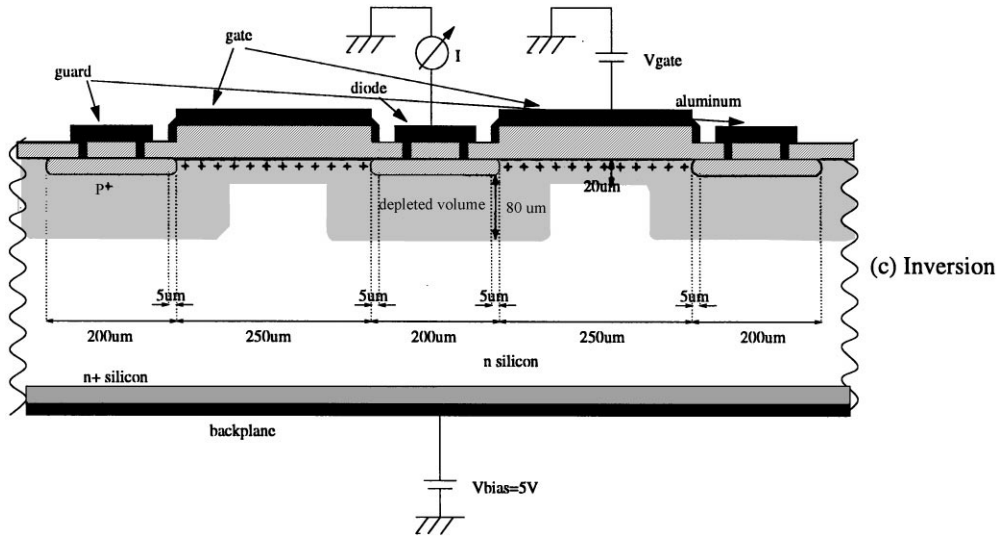


Fig. 12. Illustration of the gated diode in inversion.

isolation layer by measuring the leakage current through the double layer of SiO_2 and Si_3N_4 as function of the applied voltage.

3.4.1. Gated diode measurements

Gated diodes allow a direct measurement of contributions from surface and bulk generation to the total diode leakage current [8–10]. Fig. 12 shows a cross section through the gated diode and the connection scheme used for the measurements. The leakage current of the reversed biased diode is measured as function of the gate voltage applied to the aluminium gate surrounding the diode. A measured I - V curve with a bulk voltage of $V_{\text{bulk}} = 5 \text{ V}$ is shown in the top plot of Fig. 13. For a detailed description of gated diodes see Ref. [9].

Accumulation, depletion and inversion regions can clearly be distinguished. The accumulation plateau for $V_{\text{gate}} \geq -2.5 \text{ V}$, the depletion plateau between $V_{\text{gate}} \approx -2.5 \text{ V}$ and $V_{\text{gate}} \approx -8.0 \text{ V}$ and the inversion plateau for $V_{\text{gate}} < -8.0 \text{ V}$. Here we want to focus on the extraction of the surface generated leakage current, which is given by the current difference at the depletion and the inversion plateau. Assuming that this contribution of the diode leakage current is caused by interface states at the Si/SiO_2 interface, the measurement of the gated

diode leakage current provides a possibility to study process or radiation-induced changes of the interface state density which will be discussed in the next section.

4. Irradiation tests

4.1. Neutron irradiation

Hadronic irradiation causes bulk damage changing the effective doping concentration, N_{eff} , and leading to a fluence-proportional increase of the bulk leakage current. The change of N_{eff} can be described by a model which is based on the assumption that the concentration of donors decreases exponentially with the equivalent fluence, ϕ_{eq} , of 1 MeV neutrons due to donor-removal while at the same time acceptors are formed proportional to ϕ_{eq} [11].

The increase of the volume generation current can be described by $\Delta I = \alpha(t) \cdot \phi_{\text{eq}} \cdot V$ as function of the fluence and the bulk volume V . For the corresponding time dependence of $\alpha(t)$ we used the parameterization given in Ref. [12].

At Ljubljana, Slovenia, an unbiased detector has been exposed to a fluence of $\phi = 1 \times 10^{13} \text{ cm}^{-2}$

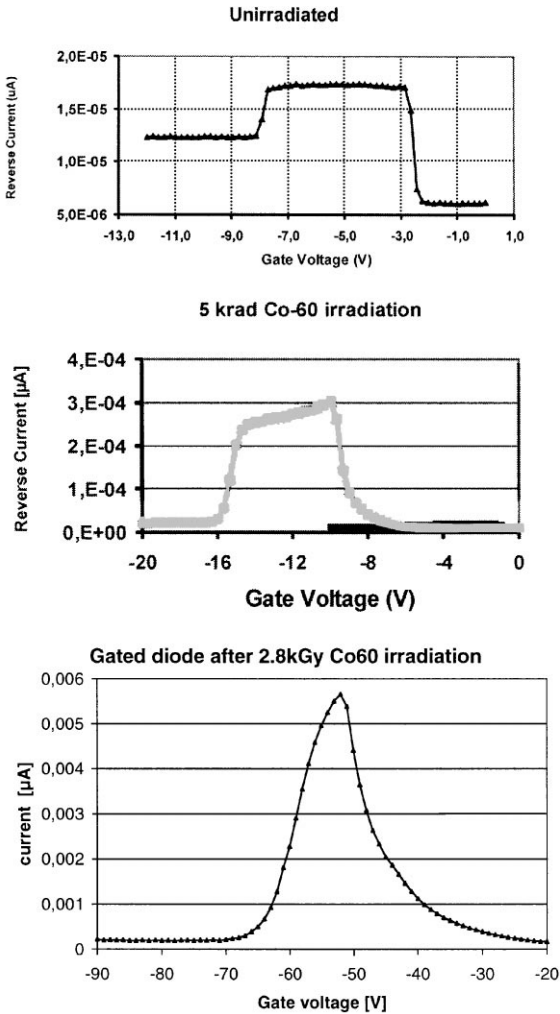


Fig. 13. I - V measurement of an unirradiated and two irradiated gated diodes.

using neutrons with an energy distribution peaking at 1 MeV. For this fluence we expected a leakage current of 546 μA after an annealing time of one week at room temperature in reasonable agreement with the measured value of 615 μA . After three weeks of annealing the measured and predicted leakage currents were $I_{\text{meas}} = 418 \mu\text{A}$ and $I_{\text{pred}} = 449 \mu\text{A}$.

For the depletion voltage, which is proportional to N_{eff} , we observed a shift from $V_{\text{dep}} = 68 \text{ V}$ to $V_{\text{dep}} = 17 \text{ V}$ and $V_{\text{dep}} = 30 \text{ V}$ after one and three weeks of annealing, respectively, while the corre-

sponding values of the prediction are $V_{\text{dep,pred}} = 28 \text{ V}$ and 27 V .

Since the results of the I - V and C - V measurements agree qualitatively with the predicted values, it is assumed that effects due to neutron radiation are under control.

4.2. γ -irradiation

Low-energy γ -irradiation tests using ^{60}Co -sources have been performed for an unbiased and a biased detector at the National Institute of Measurement at Utrecht, The Netherlands, and at the Hahn-Meitner-Institute, Berlin, Germany. At Utrecht an unbiased detector has been exposed to a radiation dose of 2 kGy at a dose rate of 62.5 Gy/h. Due to the irradiation, the dark current at $V_{\text{bias}} = 200 \text{ V}$ increased from 22 nA to 23.4 μA measured 10 h after the irradiation.

For the biased irradiation we applied a bias voltage of 100 V during radiation. The total dose was 2.8 kGy and the dose rate 150 Gy/h. Compared to the unbiased irradiation, we observed a larger increase of the leakage current. The leakage current at $V_{\text{bias}} = 200 \text{ V}$ has increased from 44 nA to 425 μA measured directly after the irradiation. After 20 h we measured a current of 280 μA one magnitude larger than the current of the unbiased irradiated detector measured after 10 h.

In order to test the annealing behaviour at room temperature, leakage currents have been measured until 25 days after the biased irradiation. After this time a decrease by a factor of 3 down to $I_{\text{leak}} = 140 \mu\text{A}$ has been observed. When scaled down linearly to a dose of 2 kGy, this value is still larger than the measured one of the unbiased irradiated detector of $I_{\text{leak}} = 12.6 \mu\text{A}$ obtained after a similar annealing time of 18 days.

Test beam measurements of neutron and γ -irradiated detectors are under way to study the detector degradation in terms of charge collection efficiency, noise and position resolution as function of incident track angles.

4.3. γ -irradiation of test structures

Each detector has been irradiated together with test structures. In the following we will report only

the main results from the γ -irradiation of the MOS capacitor and the gated diode. Since radiation effects due to ionizing radiation affect mainly oxide layers and the Si–SiO₂ interface, the large increase of the detector leakage current observed after γ -irradiations suggests the assumption that the detector leakage current is dominated by surface currents. To understand the origin of the detector leakage current after γ -irradiation we studied the characteristics of MOS capacitors and gated diodes.

4.3.1. Irradiation of MOS capacitors

As discussed above, a C – V characteristic measured at a MOS capacitance, allows the extraction of the density of charged states, located in the field oxide or in the Si–SiO₂ interface, via a measurement of the flatband voltage. Unbiased MOS capacitors have been exposed to different doses between 50 Gy and 2.8 kGy. After irradiation we have observed that both the shape of the C – V curve and the flatband voltage become frequency dependent. After 2 kGy the flatband voltage reaches values from -50 V measured at 10 kHz to -68 V measured at 120 Hz, corresponding to a large positive charge density at the oxide or Si–SiO₂ interface. Due to the irradiation the flatband voltage has been shifted by about -50 V. This shift is related to an additional amount of 1.8×10^{12} positive charges/cm².

4.3.2. Irradiation of gated diodes

The shift of the flatband voltage can be observed also on the I – V characteristics of the gated diode. The flatband voltage is strongly related to the threshold voltage, V_{th} , the value of the gate voltage, where the surface below the gate becomes inverted, resulting in the step between the depletion and inversion plateau of the I – V curve. Fig. 13 shows the I – V curve of an unirradiated and two radiated gated diodes after a dose of 50 Gy and 2.8 kGy, respectively. For radiation doses of 50 Gy and 2.8 kGy we obtained values of about $V_{th} = -15$ V and -60 V, respectively.

The I – V curves given in Fig. 13 show a strong increase of the surface current. After a dose of 50 Gy the difference between the depletion and the inversion plateau increases by a factor of 50 from

5 pA for the unirradiated diode to about 250 pA. In addition to the increase of the surface current a change of the shape of the I – V curve is observed. After 2.8 kGy the shape is strongly deformed but the bottom plot of Fig. 13 shows that the large dark current of about 5 nA is only measured in the depletion region, which allows to identify this current as a surface current.

Summarizing the measurement results obtained from the MOS capacitor and the gate diode, we conclude that high surface densities of positive charges are produced due to ionizing radiation. In addition a large increase of the surface generated leakage current is observed. Both effects, the built up of positive surface charges and the high surface leakage current could be caused by radiation-induced generation of charged interface states.

5. Summary and conclusions

The ZEUS microvertex detector is currently under construction. A test program is under way to understand the main performance and main characteristics of the silicon strip detectors. Test beam measurements have shown that the predicted position resolution of about 7.5 μ m has been achieved. Distributions of the detector leakage current and the depletion voltage obtained from quality-control measurements are presented. The leakage currents of the delivered detectors are typical about 30–50 nA and values of the full depletion voltage are between 40 and 65 V. The long-term stability of each detector is measured in a test, where the detector leakage current at $V_{bias} = 200$ V is monitored for 42 h. First results have shown that the number of detectors not accepted for assembling is below 1%. Test structure measurements have been used for radiation studies and for the control of process parameters, which are found to be within the specifications. Large surface leakage currents and high densities of surface charges are observed after γ -irradiation of MOS capacitors and gated diodes, indicating high densities of radiation induced interface states. Detectors, exposed to neutron and γ -irradiation show leakage currents of several microamps, 3–4 magnitudes above the values of unirradiated detectors. Leakage currents

measured after γ -irradiation are about one magnitude higher if detectors are biased during irradiation, compared to unbiased irradiations. Test beam measurements of irradiated detectors have been started. The installation of the microvertex detector inside ZEUS is foreseen during the shutdown starting in year 2000.

Acknowledgements

I would like to thank my colleagues from the ZEUS MVD – group on whose work this talk is based and the members of the Hamamatsu solid state department for the excellent collaboration.

References

[1] ZEUS Collab., M. Derrick et al., The ZEUS Detector, Status Report 1993, DESY, 1993.

- [2] U. Schneekloth (Ed.), The HERA Luminosity Upgrade, DESY HERA 98-05, 1998.
- [3] A Microvertex Detector for ZEUS, ZEUS-Note 97-006, 1997.
- [4] F. Feuerstack-Raible et al., Second Workshop on Electronics for LHC Experiments, Balatonfüred, Hungary, September 1996.
- [5] K. Riechmann, Nucl. Instr. and Meth. A 408 (1998) 221.
- [6] A. Garfagnini, Nucl. Instr. and Meth. A 435 (1999) 34.
- [7] B. England et al., Nucl. Instr. and Meth. A 235 (1985) 481.
- [8] T. Johnsen, Thesis submitted for the degree of Candidatus Scientiarum at the University of Bergen, Department of Physics, Oslo, June 1994.
- [9] A.S. Grove, Physics and Technology of Semiconductor Devices, Wiley, New York, 1967.
- [10] G. Vanstraelen et al., Nucl. Instr. and Meth. A 288 (1990) 48.
- [11] G. Lindström, M. Moll, E. Fretwurst, Nucl. Instr. and Meth. A 426 (1999) 1.
- [12] M. Moll, Ph.D. Thesis, University Hamburg, 1999.